Resolving Magnetopause Shadowing Using Multi-Mission Measurements of Phase Space Density

Frances A Staples[1], Adam C Kellerman[2], Kyle Robert Murphy[3], I. Jonathan Rae[4], Jasmine Kaur Sandhu[4], and Colin Forsyth[5]

[1]Mullard Space Science Laboratory
[2]University of California Los Angeles
[3]University of Maryland/NASA Goddard
[4]Northumbria University
[5]University College London

November 24, 2022

Abstract

Loss mechanisms act independently or in unison to drive rapid loss of electrons in the radiation belts. Electrons may be lost by precipitation into the Earth's atmosphere, or through the magnetopause into interplanetary space; a process known as magnetopause shadowing. Whilst magnetopause shadowing is known to produce dropouts in electron flux, it is unclear if shadowing continues to remove particles in tandem with electron acceleration processes, limiting the overall flux increase. We investigated the contribution of shadowing to overall radiation belt fluxes throughout a geomagnetic storm starting on the 7 September 2017. We use new, multi-spacecraft phase space density calculations to decipher electron dynamics during each storm phase and identify features of magnetopause shadowing during both the net-loss and the net-acceleration storm phases. We also highlight two distinct types of shadowing; 'direct', where electrons are lost as their orbit intersects the magnetopause, and 'indirect', where electrons are lost through ULF wave driven radial transport towards the magnetopause boundary.

Resolving Magnetopause Shadowing Using Multi-Mission Measurements of Phase Space Density

F. A. Staples[1], A. Kellerman[2], K. R. Murphy[3], I. J. Rae[4], J. K. Sandhu[4], C. Forsyth[1]

[1]Mullard Space Science Laboratory, University College London, London, UK.

[2]Department of Earth, Planetary, and Space Sciences, University of California, Los Angeles, USA.

[3]NASA Goddard Space Flight Centre, Greenbelt, MD, USA.

[4]Northumbria University, Newcastle upon Tyne, UK.

Corresponding author: Frances A. Staples (frances.staples@ucl.ac.uk)

Key Points:

- Multi-point phase space density measurements resolve changes in relativistic electron flux on sub-hour timescales.
- We observed magnetopause shadowing loss and localized electron acceleration during the September 2017 geomagnetic storm.
- 'Direct' and 'indirect' magnetopause shadowing processes identified during both the net-loss and net-acceleration phases of the storm.

Abstract

Loss mechanisms act independently or in unison to drive rapid loss of electrons in the radiation belts. Electrons may be lost by precipitation into the Earth's atmosphere, or through the magnetopause into interplanetary space – a process known as magnetopause shadowing. Whilst magnetopause shadowing is known to produce dropouts in electron flux, it is unclear if shadowing continues to remove particles in tandem with electron acceleration processes, limiting the overall flux increase. We investigated the contribution of shadowing to overall radiation belt fluxes throughout a geomagnetic storm starting on the 7 September 2017. We use new, multi-spacecraft phase space density calculations to decipher electron dynamics during each storm phase and identify features of magnetopause shadowing during both the net-loss and the net-acceleration storm phases. We also highlight two distinct types of shadowing; 'direct', where electrons are lost as their orbit intersects the magnetopause, and 'indirect', where electrons are lost through ULF wave driven radial transport towards the magnetopause boundary.

Plain Language Summary

Charged particles with extremely high energies are trapped by Earth's geomagnetic field. These particles form rings around Earth called the Van Allen radiation belts, which vary in intensity. This radiation poses a risk to satellites orbiting Earth, so it is important to understand how changes in geomagnetic conditions produce variations in the radiation belt intensity. In this work we take measurements of electron radiation from many satellites to observe electron 'dropouts', where nearly the entire radiation belt is lost in a matter of hours. We found that it is necessary to use multi-mission measurements to make observations of dropouts because a dropout may occur quicker than a single satellite can traverse the radiation belt. In early September 2017, we observed that movements of the geomagnetic outer boundary, the magnetopause, was responsible for removing electrons, combined with diffusive processes. This agreed with the predictions by previous studies. We further observed that the magnetopause continued to remove electrons from the belt whilst electrons were simultaneously accelerated by fluctuations in the geomagnetic field. This is significant because electrons may be removed from the belt soon after they were created, limiting the overall growth of the radiation belt whilst the magnetopause was compressed.

1 Introduction

The outer radiation belt is a ring of relativistic electrons which are trapped by Earth's magnetosphere, surrounding the Earth at distances from ~3 to 8 Earth Radii above Earth's surface. This population of particles has a range of energies between hundreds of keV to tens of MeV (Mauk et al., 2013), which can pose a hazard to the operation of satellites which lie within the belt (e.g., Baker et al., 1994; Wrenn, 1995; Wrenn et al., 2002). Most of the time, the outer belt is slowly varying, however, during geomagnetic storms the particle flux in the outer belt by change by orders of magnitude in a matter of hours to days (e.g. Baker et al., 1994; Morley et al., 2010). Furthermore, a geomagnetic storm may result in a net-increase, decrease, or no response in radiation belt flux (Reeves et al., 2003). Continuously competing acceleration and loss mechanisms, which act to create or remove relativistic electrons from the magnetosphere, determine the net flux of electrons in the outer belt.

Acceleration of electrons can occur via gyro-resonant wave-particle interactions between 100's of keV 'seed' electrons and very low frequency (VLF) whistler mode waves (Baker et al., 1998; Horne et al., 2005; Meredith et al., 2002; Summers et al., 1998). Particles may also be

energized by drift-resonant wave particle interactions with ultralow frequency (ULF) waves (e.g., Elkington et al., 1999; Mann et al., 2013), or by ULF driven inwards radial diffusion (e.g., Fälthammar, 1965; Jaynes et al., 2015). This inward diffusion of electrons results in betatron acceleration which energizes electrons. Similarly, electrons are decelerated if they are transported outwards via radial diffusion. If the ring current is enhanced, electrons may also be adiabatically transported outwards, and decelerated (Dessler & Karplus, 1961; McIlwain, 1966).

Loss mechanisms act independently or in unison to remove electrons from the radiation belts. Electrons are either lost by precipitation into the atmosphere, induced by wave-particle interactions resulting in pitch-angle scattering (e.g., Miyoshi et al., 2008; Rae et al., 2018; Rodger et al., 2015; Thorne & Kennel, 1971), or through the magnetopause into interplanetary space. The latter process is called magnetopause shadowing, and electrons are either lost directly to the compressed magnetopause intersecting drift paths (direct shadowing) (Green et al., 2004; Kim et al., 2008; Li et al., 1997; Saito et al., 2010) or indirectly if electrons are transported towards the magnetopause boundary and subsequently lost (Brautigam & Albert, 2000; Loto'aniu et al., 2010; Morley et al., 2010; Rodger et al., 2019; Shprits et al., 2006; Turner et al., 2012).

Geomagnetic storms produce highly variable electron fluxes because both acceleration and loss mechanisms are enhanced, acting in separate locations and on a variety of timescales. It is understood that the radiation belts have a two-step response to geomagnetic storms; a net-loss phase when the radiation belt flux decreases overall during storm onset, followed by a net-acceleration phase where radiation flux increases overall (Murphy et al., 2018). Electrons are usually lost from the belts before lower energy electrons are accelerated because of the way in which the magnetosphere responds to solar wind structures which drive geomagnetic storms. At storm onset, the magnetopause is often compressed by shock structures in the solar wind (e.g. Dmitriev et al., 2014; Sibeck et al., 1989), resulting in some loss of electrons via magnetopause shadowing. If the compression is large enough, losses due to shadowing are extreme, and the entire outer radiation belt may suddenly decrease by orders of magnitude over a timescale of hours; this is referred to as a dropout (e.g. Borovsky et al., 2009; Onsager et al., 2002). Dropouts are important precursors to the latter net-acceleration phase as they remove both the existing radiation electrons and seed electrons, which limits the number of particles accelerated from this lower energy population (Bingham et al., 2018). The resulting net-loss period may extend into main phase of the geomagnetic storm, then acceleration mechanisms begin to increase the overall

electron flux. The net-acceleration phase is delayed compared to the net-loss phase because the timescales of wave driven acceleration and/or ULF driven diffusion is slower (hours to days) (Baker et al., 1994; Boyd et al., 2014; Elkington et al., 2003; Horne et al., 2005; Reeves et al., 2013). It is not known whether magnetopause shadowing continues to contribute to the overall flux during the net-acceleration phase.

Because of the fast nature of shadowing, it is extremely hard to study the characteristics of dropout events in detail. So far, magnetopause shadowing observations include identifications of simultaneously compressed magnetopause and a net-decrease in electron flux (e.g., Morley et al., 2010; Rodger et al., 2019) and/or measurements of butterfly pitch angle distributions near the compressed magnetopause (e.g., Kang et al., 2018; Ozeke et al., 2020; Tu et al., 2019). Such pitch angle distributions are an observational feature of shadowing since equatorial bouncing particles (with a high pitch angle) drift to higher radial distances at the magnetopause nose than high latitude bouncing particles (with low pitch angles), therefore high pitch angle electrons are preferentially lost to the magnetopause (Sibeck et al., 1987).

It is thought that magnetopause shadowing will have specific characteristics identifiable in phase space density (PSD) (Green & Kivelson, 2004; Loto'aniu et al., 2010; Turner et al., 2012). The collective dynamics of the radiation belts are often determined by using measurements of PSD, transformed into adiabatic invariant space μ, K, and L*. Radiation belt studies have notably used PSD to distinguish localized internal sources of high energy electrons (e.g. Boyd et al., 2014; Chen et al., 2006; Green & Kivelson, 2004; Miyoshi et al., 2003; Selesnick & Blake, 2000) from radial diffusion of an external source (e.g. Degeling, 2008; Jaynes et al., 2018; Ozeke et al., 2019).

In order to discern the physical processes occurring during storm times, Turner et al. (2012) presented a schematic of PSD evolution, as a function of L*, during a direct magnetopause shadowing event that results in a dropout (Figure 3, Turner et al., 2012). There is an initial ‘high pressure’ phase during storm onset where the outer boundary of the radiation belt is compressed such that a significant amount of the PSD distribution is lost to interplanetary space. When the pressure relaxes during the main storm phase, the magnetopause expands and there is a peak in PSD at the minimum radial distance which the magnetopause reached during the compression, and a strong negative gradient in PSD towards the expanded magnetopause.

Over time, ULF wave activity during the main phase of the storm will rapidly diffuse the remaining particles down any radial gradients in the PSD profile, resulting in a decrease in the L* location of peak PSD, and a decrease in PSD at all L* compared to the pre-storm distribution. Furthermore, in Figure 1 of Loto'aniu et al. (2010), the authors presented another scenario where a combined negative phase space density gradient and enhanced ULF wave activity will lead to indirect magnetopause shadowing.

Whilst PSD has been used to analyze electron dropouts (e.g., Ma et al., 2020; Shprits et al., 2012; Turner et al., 2013; Xiang et al., 2017; Zou et al., 2020), the stages of magnetopause shadowing described by Turner et al. (2012) has not yet been explicitly identified using PSD measurements. This is because dropouts occur on such fast timescales that it is difficult to measure complete PSD profiles in L* on the timescales necessary for this observation with single or even dual spacecraft in geostationary transfer orbits. In this study we investigate the dynamics of PSD during the early September 2017 geomagnetic storm using a new multi-spacecraft dataset of PSD measurements that covers L* = 1.5 to 9. By using a multi-satellite dataset, we can measure PSD with high enough temporal and spatial resolution to investigate whether the Turner et al. (2012) description of a magnetopause shadowing event is accurate.

2 Data

2.1 Phase Space Density Measurements

In this paper, we primarily use Phase Space Density (PSD) to characterize the radiation belt response to a geomagnetic storm from 7-10 September 2017. PSD describes the kinematical state of radiation belt electrons using three coordinates of position, and the three components of canonical momentum (Schulz and Lanzerotti, 1974). Since the number of electrons in the radiation belt is sufficiently large and energetic, we can describe gyration, bounce, and drift motions in terms of three adiabatic invariants of motion, namely μ, K, and L* (Roederer, 1970). In this formalism we consider only the phase-averaged motion of particles, reducing the problem to a three-dimensional approximation of the system. We then consider the density of electrons in this phase space, the PSD.

The benefit of using an invariant PSD is that non-adiabatic processes are easily identified by any changes to the PSD distribution; that is, the PSD distribution does not change if only adiabatic changes are occurring to the system (following Liouville's theorem). Furthermore, the PSD distribution in L* is an important characteristic when interpreting indirect magnetopause shadowing processes because the PSD gradient in L* determines the rate of particle diffusion towards this outer boundary.

The electron PSD is here defined in units of (c/cm/MeV)3, following the Committee on Space Research (COSPAR) Panel on Radiation Belt Environment Modelling (PRBEM) recommendations. For each spacecraft and instrument, the adiabatic invariants μ, K, and L* (Roederer, 1970) are computed using the International Radiation Belt Models (IRBEM) library (Boscher, 2013), the International Geomagnetic Reference Field (IGRF) internal field model, and the semi-empirical Tsyganenko 2001 storm (T01s) external magnetic field model (Tsyganenko et al., 2003). Through the September 2017 storm we use PSD measurements from;

- Van Allen Probes MagEIS (Magnetic Electron Ion Spectrometer) and REPT (Relativistic Eletron-Proton Telescope) instruments (Mauk et al., 2013; Blake et al., 2012; Baker et al., 2013),

- THEMIS ESA (Electrostatic Analyzer) and SST (Solid State Telescope) instruments (Angelopoulos, 2009; Angelopoulos et al., 2008; McFadden et al., 2008),
- MMS FEEPS (Fly's Eye Electron Proton Spectrometer) instrument (Blake et al., 2016; Burch et al., 2016),
- GOES MAGED (Magnetospheric Electron Detector) and EPEAD (Energetic Proton, Electron, and Alpha Detector) (GOES N Series Data Book, 2010; Hanser, 2011; Rodriguez et al., 2014),
- GPS (Global Positioning System) Navstar Satellite CXD (Combined X-Ray Dosimeter) (Tuszewski et al., 2004).

Each instrument is cross calibrated with the Van Allen Probe B MagEIS measurements.

Rather than interpolating PSD observations to find PSD for specific μ and K, as is traditionally practiced, in this study we use PSD measurements which lie within a specified range of μ and K to represent a specific population of electrons. For μ we use a range of ± 2.5%; e.g., for a specified mu of 400 MeV/G, the range is 390 - 410 MeV/G. The range of K used is ± 25%; e.g., for a specified K 0.1 G0.5RE, the range is 0.75 to 1.25 G0.5RE. A relatively large range of K was chosen in order to maximize the PSD data available in each distribution across all L*, whilst a small μ range was chosen to limit any overlap between measurements taken by different energy channel ranges for different satellites.

2.2 Parameterisation of the Outer Boundary

In this study we use both measurements of the magnetopause and calculations of the last closed drift shell (LCDS) when considering the outer boundary of the radiation belts. We calculate the LCDS numerically as the maximum L* at which an electron with a given pitch angle follows a closed drift path in the T01s external magnetic field model, where there is a single magnetic minima along a field line. The magnetopause location is represented by the Shue et al. (1998) magnetopause model, and by measurements of the magnetopause location taken by the THEMIS and GOES spacecraft. We supplement the Shue et al. (1998) model with magnetopause measurements as it has been shown that

200 statistical models may not reflect event specific behavior of the magnetopause location
201 during dynamic magnetopause compressions (Staples et al., 2020). To identify THEMIS
202 magnetopause crossings, magnetic and plasma measurements are taken from the Fluxgate
203 magnetometer (Auster et al., 2008) and the Electrostatic Analyzer (McFadden et al.,
204 2008). For GOES 13 and 15 magnetopause crossings, magnetic field data from the flux
205 gate magnetometers was used (Singer et al., 1996).

206 2.3 Solar Wind Data

207 Solar wind data and geomagnetic indices used are provided by the
208 NASA/Goddard Space Flight Centers OMNI data set through Coordinated Data Analysis
209 Web (CDAWeb; https://omniweb.gsfc.nasa.gov/). Solar wind measurements in this
210 dataset are taken by the ACE, Wind, IMP 8, and Geotail missions, and are propagated to
211 the bow shock nose. The SYM-H index, calculated in a similar manner to Dst index by
212 ground based midlatitude magnetometer stations, is used to indicate geomagnetic activity
213 (Iyemori, 1990; Iyemori et al., 2010; Wanliss et al., 2006). All data used from CDAWeb
214 has 5-minute resolution.
215

3 Results

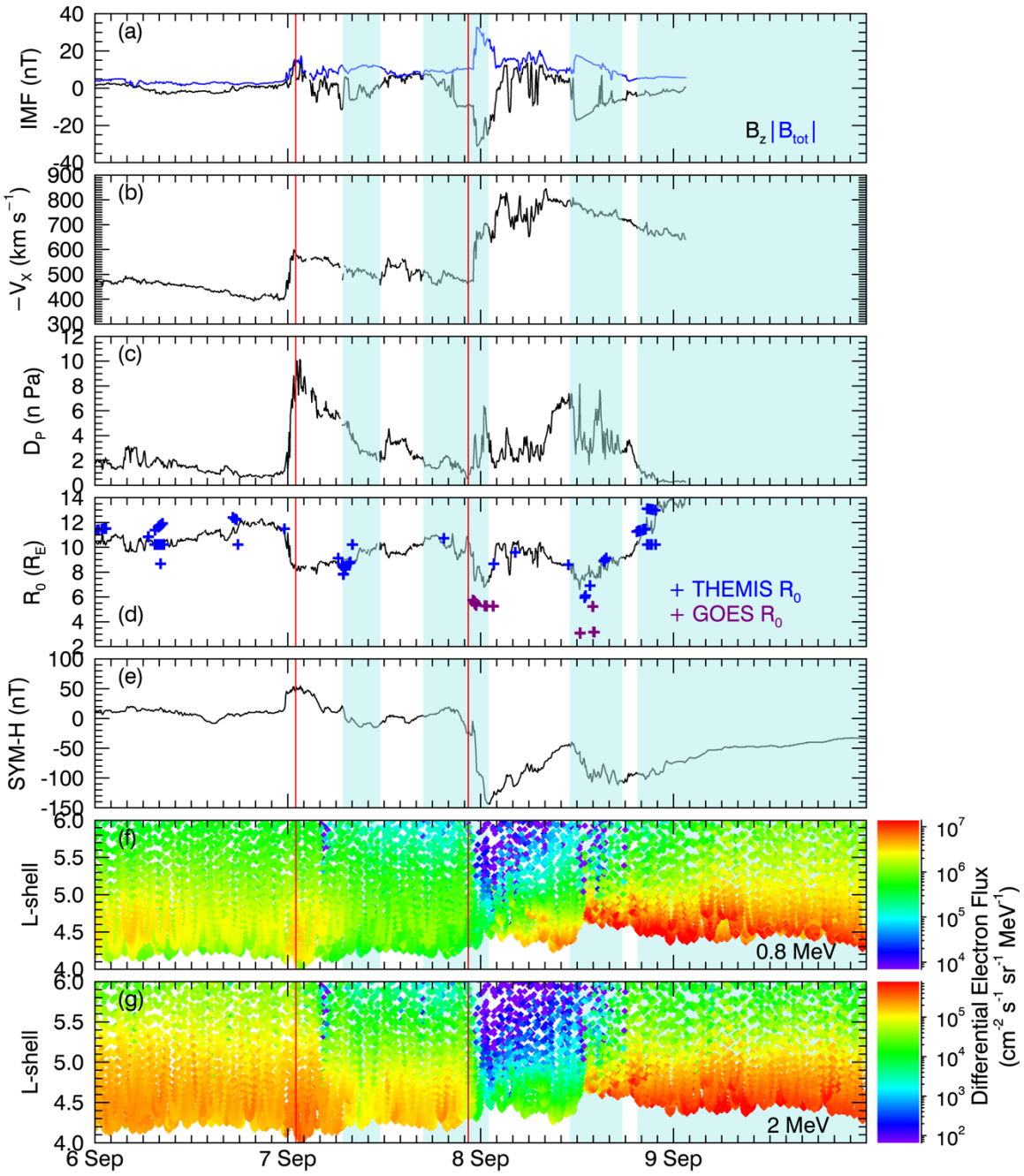

Figure 1. The solar wind and magnetospheric conditions for the 6 - 10 September 2017; (a) total IMF (blue) and the north-south component of IMF BZ (black); (b) solar wind speed; (c) solar wind dynamic pressure; (d) subsolar standoff distance of the magnetopause, calculated by the Shue et al. (1998) model (black line), and equivalent subsolar standoff distance measured by

222 THEMIS (blue) and GOES (purple) spacecraft according to Staples et al. (2020); (e) SYM-H
223 index; differential electron flux as a function of L shell, measured by GPS satellites at (f) 0.8
224 MeV and (g) 2 MeV. Interplanetary shocks are indicated by red lines and blue shaded areas show
225 when there are CME ejecta as stated by Shen et al., (2018).

226

227 Figure 1 shows a summary of solar wind, interplanetary magnetic field (IMF),
228 magnetospheric parameters, and radiation belt electron flux between the 6 - 10 of September
229 2017. During the time period there is a complex sequence of interacting interplanetary shocks
230 and coronal mass ejecta (CME) (Scolini et al., 2020; Shen et al., 2018; Werner et al., 2019)
231 which drives an equally complex magnetospheric and radiation belt response. The times of the
232 interplanetary shocks and CME ejecta classified by Shen et al. (2018) are displayed by the red
233 lines and blue shaded areas respectively. Measurements of electron flux at 0.8 MeV and 2 MeV
234 energies are taken by the combined X-ray dosimeter on board LANL GPS Navstar satellites
235 (Tuszewski et al., 2004). As the orbits of GPS satellites are highly inclined, measurements of
236 flux at L shells $\gtrsim 5.5$ are taken at high magnetic latitudes where fewer electrons complete their
237 bounce orbit, and therefore flux decreases rapidly with L shell.

238 The arrival of the first interplanetary shock is indicated by an increase in solar wind
239 speed (Figure 1b) and dynamic pressure (Figure 1c) by 200 kms-1 and 9 nPa respectively, and an
240 increase in IMF strength by 15 nT (Figure 1a). At 01:00 UT on 7 September 2017, the increased
241 dynamic pressure resulted in a compression of the magnetopause from 11.5 RE to 8 RE (Figure
242 1d), and an increase in SYM-H index from ~ 10 nT to 50 nT (Figure 1e) as magnetopause
243 currents are enhanced by the increased solar wind number density (not shown). Both 0.8 MeV
244 and 2 MeV flux increased by a factor of ~2 at all L shells < 5 (figure f-g). When SYM-H index
245 returned to the pre-storm value of ~ 10 nT, so did electron flux at both energies.

246 The first CME ejecta arrived at 06:50 UT 7 September, accompanied by an IMF BZ
247 rotation, increasing from -10 nT to 9 nT then decreasing to – 8 nT (Figure 1a), and there is an
248 overall decrease in solar wind velocity and dynamic pressure (Figures 1b & 1c respectively).
249 There is no significant change in SYM-H as it returned to ~ 0 nT prior to the first ejecta (Figure
250 1e). The magnetopause began to expand outwards from 8 RE to 10 RE, with THEMIS measuring
251 the equivalent subsolar magnetopause between 8 and 10 Re during this period (Figure 1d).

Electron flux decreased by a factor of ~4 compared to the pre-storm flux, for both energies, and at all L shells (Figure 1f-g).

The second CME arrived at 16:50 UT 7 September and lasted until 01:00 UT 8 September. A second interplanetary shock which (was associated with the third CME) was propagating within this second CME ejecta, and arrived at 22:28 UT 7 September. When the second CME ejecta arrived at 16:50 UT 7 September, solar wind speed and pressure continued to decrease gradually (Figure 1b & c respectively), and IMF BZ decreased from 8 nT to –10 nT (Figure 1a). Interestingly, the magnetopause did not change location significantly (Figure 1d), there was no geomagnetic activity (Figure 1e), and no change to electron fluxes (Figure 1f-g). However, when the interplanetary shock arrived, IMF field strength suddenly increased from 10 nT to ~35 nT and BZ decreased further from –10 nT to –32 nT. Solar wind speed increased from 500 kms-1 to 700 kms -1, and dynamic pressure increased from 1 nPa to 4 nPa. The magnetopause was compressed within geostationary orbit (~6.6 RE) where there were multiple magnetopause crossings by GOES 13. The Shue et al. (1998) magnetopause model calculated a minimum standoff distance of 7 RE, whereas the equivalent standoff distance calculated for the GOES magnetopause crossings is 5.5 RE. The SYM-H index decreased from 0 nT to a minimum of –142 nT following the shock. The 0.8 MeV electron flux decreased by a factor of ~ 100 across L shells > 5 and ~ 10 for L shells < 5. Similarly, 2 MeV electron flux also decreased following the interplanetary shock, but by a factor of ~1000 for L shells > 5 and a factor of ~100 at L shells < 5. At both energies, this dropout in flux started at the highest L shells first, followed by the lower L shells over a 3-hour time period.

Following the second CME ejecta solar wind speed remains high at 800 km s-1 (Figure 1b), whilst dynamic pressure fluctuated, increasing from 1 nPa to 6 nPa (Figure 1c). IMF BZ also fluctuated rapidly between –10 nT and 10 nT (Figure 1a). SYM-H began to increase (Figure 1e), indicating that the start of the storm recovery phase. The magnetopause expanded outwards to ~ 10 RE, as measured by THEMIS (Figure 1d). Electron flux increased across both energies; 0.8 MeV flux increased by a factor of $\gtrsim 10$, first limited to L shells < 4.5 but slowly expanding to all L shells prior to the third CME arrival (Figure 1f). The 2 MeV electrons showed a similar increase in flux, though the rate of increase was slower (Figure 1g).

281 The third CME ejecta arrived on 8 September at 11:05 UT and lasted until 17:38 UT.
282 Solar wind speed remained high at 800 kms-1, decreasing to 700 km/s through the ejecta (Figure
283 1b), and solar wind pressure fluctuated rapidly between 2 and 8 nPa (Figure 1c). IMF strength
284 suddenly increased by 8 nT, and BZ rapidly decreased to –10 nT, both field strength and BZ
285 slowly returned to ~ 0 nT by the end of the CME (Figure 1a). SYM-H index decreased from –50
286 nT to a minimum of –120 nT (Figure 1e). The magnetopause was compressed within GEO orbit,
287 as measured by GOES 13 and 15 magnetopause crossings (Figure 1f). The Shue et al. (1998)
288 model is compressed to 7 RE at the subsolar point, and the equivalent subsolar magnetopause
289 calculated from GOES 13 crossing was 5.5 RE, and 3 RE for GOES 15. In actuality, the
290 magnetopause is not compressed to this level at the subsolar point as Van Allen Probe A is at
291 apogee near noon at this time and does not cross the magnetopause. Simultaneous to the
292 compression of the magnetopause, there is a sudden increase in flux for L shells < 5; the 0.8
293 MeV increased by a factor of ~ 10 and 2 MeV flux increased by a factor of ~ 100 (Figure 1f-g).
294 At L shells > 5 there is some reduction in flux, at both energies, compared to the flux at the
295 beginning of the third CME.

296 The fourth CME ejecta arrived at 19:30 UT 8 September and continued until 00:00 UT
297 11 September. Solar wind conditions are no longer recorded in the 5-minute resolution OMNI-
298 database during this period (Figure 1a-c). The magnetopause expanded to 13.5 RE, as measured
299 by THEMIS on 8 September (Figure 1d). For the remainder of the time period, electron flux at
300 both energies, and all L shells, continued to increase to values ~ 10 times greater than the pre-
301 storm flux (Figure 1f-g). The SYM-H index slowly increased during the recovery phase of the
302 storm (Figure 1e).

303

304

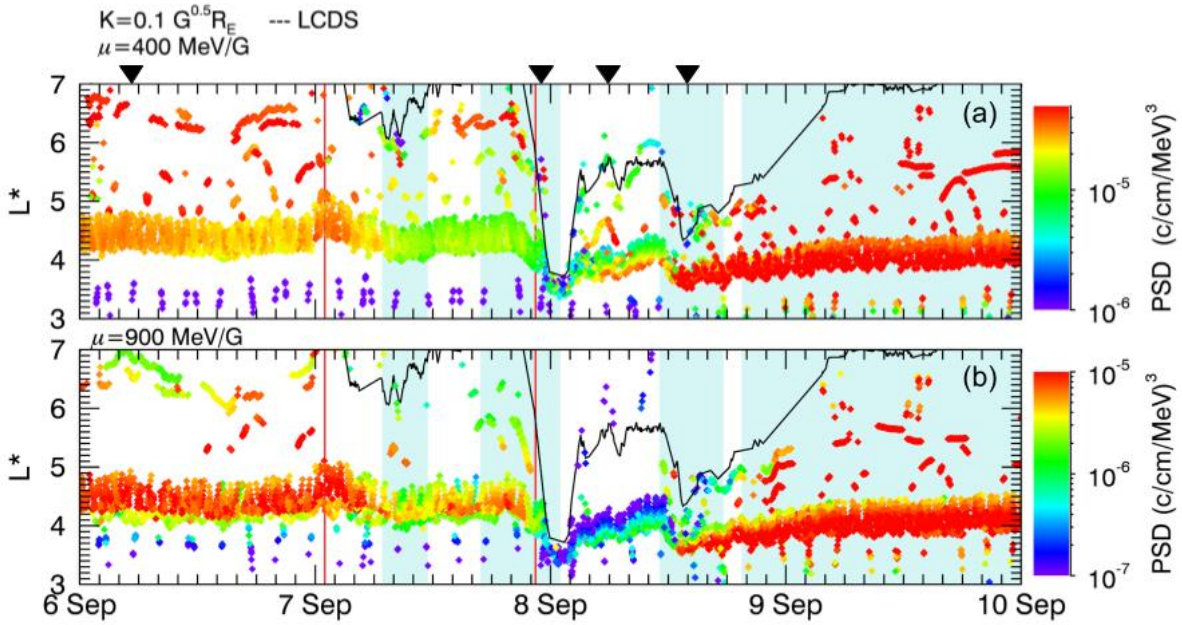

Figure 2. Phase Space Density shown as a function of L* over time as measured by multiple spacecraft for 6 - 10 September 2017; panels show PSD values where K=0.1 G0.5 RE and μ is (a) 400 MeV/G; (b) 900 MeV/G. Interplanetary shocks are indicated by red lines, and blue shaded areas show when there are CME ejecta as stated by Shen et al. (2018). The LCDS for K = 0.1 G0.5 RE is overplotted in the black solid line on all three panels. The black triangles indicate the time periods depicted in Figure 3.

Figure 2 shows PSD of electrons measured by Van Allen Probes, THEMIS, MMS, GOES, and GPS. The evolution of PSD where K=0.1 G0.5 RE and μ is 400 MeV/G and 900 MeV/G (panels a and b respectively) is shown as a function of L*. As with Figure 1, solar wind features are indicated by the red lines (interplanetary shocks) and blue shaded regions (CME ejecta).

At the beginning of 6 September, PSD increased rapidly with increasing L* up to L* = 4 for μ = 400 MeV/G, or L* = 4.2 for μ = 900 MeV/G, then increased more slowly with L* beyond that. PSD where μ = 400 MeV/G increased from 1 x10-6 to ~1.2 x10-5 (c/cm/MeV)3 at 3 < L* < 4. At L* > 4, PSD slowly increased with increasing L* from ~1.2 x10-5 to 1.3 x10-5

(c/cm/MeV)3. PSD at μ = 900 MeV/G increased rapidly from ~ 1.0 x10-7 to 1.6 x10-6 (c/cm/MeV)3 between 3 < L* < 4.2, PSD was approximately constant between 4.2 < L* < 5, and at L* > 6 PSD was between 1.4 x10-6 and 1.0 x10 -6 (c/cm/MeV)3, indicating that PSD decreased at high L*. The LCDS was beyond L* of 7, so was not plotted for this time period.

When the first interplanetary shock reached the magnetosphere, the location of spacecraft measurements in L* increased briefly, this indicated that drift paths of electrons moved Earthwards with respect to spacecraft orbits (Figure 2; red line). There were no large changes to the PSD distribution in L* for μ = 900 MeV/G, however the PSD of the 400 MeV/G population doubled. As L* returned to the pre-shock location, the increased PSD returned to the level prior to the interplanetary shock arrival. Simultaneously the LCDS moved inwards to 6.3 L*.

When the first CME ejecta reached the magnetosphere at 06:50 UT on 07 September, the LCDS moved inwards to L* ~ 6. PSD decreased across all μ, though these decreases in PSD were not uniform across L* and energies. PSD of the μ = 400 MeV/G population decreased by half between 4 < L* < 5, and by a factor of ~3 at L* >5. PSD of electrons with μ = 900 MeV/G decreased by a factor of ~5 between 4 < L* < 5 and decreased by a factor of ~3 between 3 < L* < 5.

The second interplanetary shock arrived during the third CME ejecta. In response, the LCDS was compressed to L* = 3.8 for 2 hours. The PSD at L* > 3.8 could therefore not be expressed in adiabatic coordinates during this time, so we assume these particles no longer followed closed drift paths. At locations within the LCDS, the location of spacecraft measurements in L* decreased. PSD at a given L* did not change significantly for μ = 900 MeV/G during this time period. PSD where μ = 400 MeV/G increased by a factor of ~2 at L* > 3.2 compared to corresponding measurements prior to the compression.

During the interval between the second and third CME ejecta, the LCDS expanded to higher L* of ~ 5.5. In tandem, the location of spacecraft measurements in L* moved outwards (so electron drift paths move inwards with respect to spacecraft orbits). Initially there was little to no change in PSD for μ = 400 MeV/G at a given L*, then PSD increased by a factor of 10 over the interval for L* ~ 4. At both μ = 900 MeV/G, PSD decreased by a factor of 10 compared to PSD prior interplanetary shock arrived. Through the remainder of the interval PSD increased

by a factor of ~10 at L* ~ 4. Note that for both μ, the latter increase in PSD is limited to L*~4, and PSD at L* > 4 did not increase.

Upon the arrival of the third CME ejecta, the LCDS was compressed a second time to L* = 4.4. Simultaneously, PSD at both μ increased by a factor of 10 at L* = 3.6, and PSD decreased with increasing L*. As the LCDS began to expand outwards in L*, PSD began to increase at all L*. When the fourth CME ejecta arrived, the LCDS continued to expand to higher L*, and PSD universally increased at all L* and μ plotted.

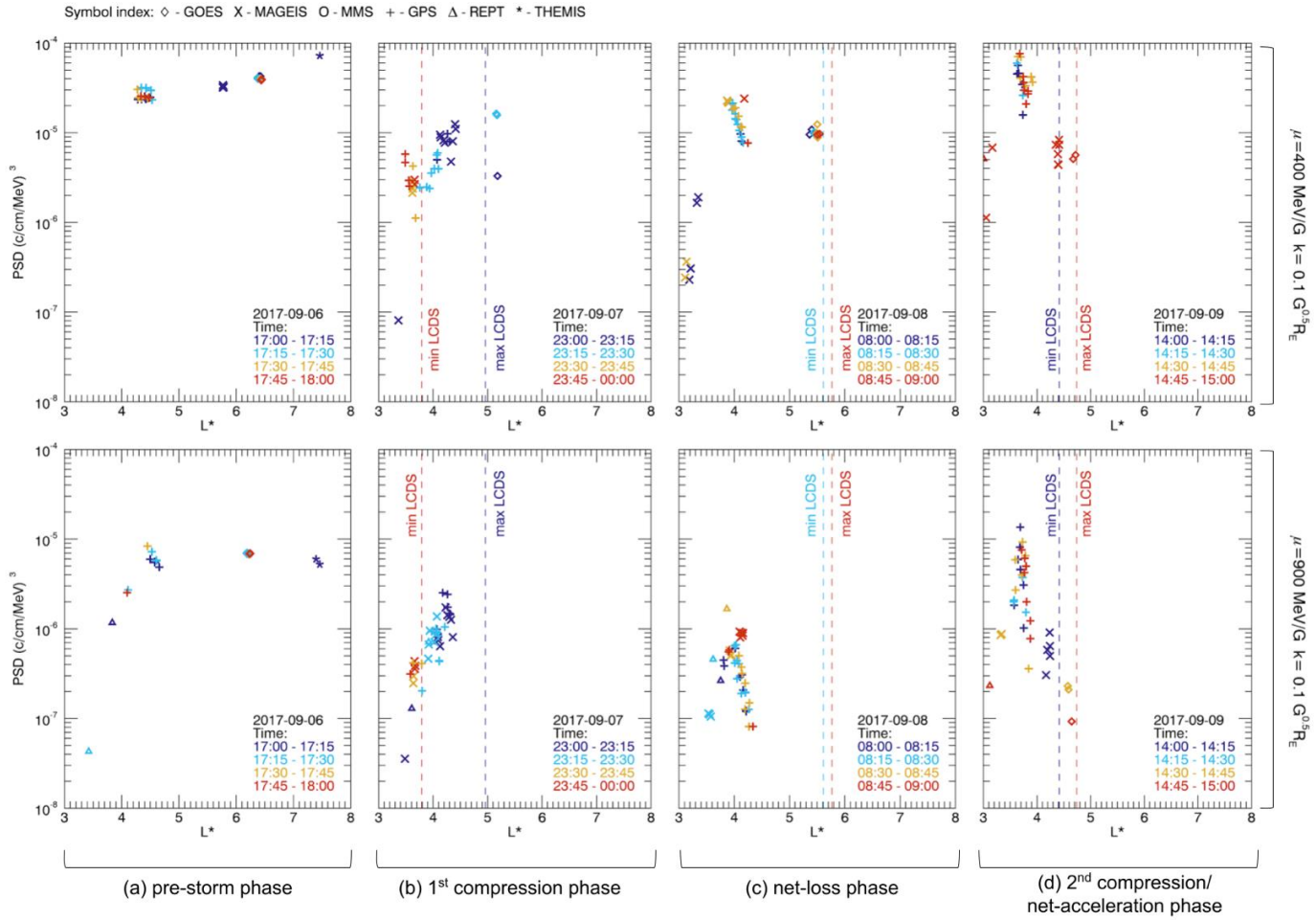

Figure 3: PSD profiles in L* for μ of 400 MeV/G (top row) and 900 MeV/G (bottom row) with K = 0.1 G0.5RE. Each column (a-d) shows a single hour time period through different phases of the storm. Symbol colors indicate when measurements were taken within the hour period. Dotted lines show the minimum and maximum L* of the LCDS.

In order to evaluate whether the Turner et al. (2012) representation of magnetopause shadowing in PSD profiles is accurate for this storm, we selected four different 1-hour time periods throughout the September 2017 storm and created PSD profiles in L*, shown in Figure 4. We selected time periods by considering the phase of the storm (i.e., pre storm, net-loss, or net-acceleration), the data availability of PSD measurements, and whether there were coinciding magnetopause measurements to define the outer boundary. The four time periods correspond to (a) pre-storm, (b) first compressive phase, (b) net-loss phase, and (c) second compressive/net-acceleration phase. Within the hour time periods 15-minute intervals are identified by symbol color so that changes to PSD and the LCDS within the hour can be identified. To give the four 1-hour time periods in the context of the storm as a whole, the time intervals are indicated by black triangles in Figure 2.

Prior to the arrival of the first interplanetary shock, Figure 3a shows PSD at both μ increased rapidly between $3 < L^* < 4.2$. Where μ = 400 MeV/G, PSD continued to increase with increasing L*, reaching maximum measurement of 1.8 x10-5 (c/cm/MeV)3 at L*= 7.4. Where μ = 900 MeV/G the maximum measured PSD was 1.0x10-5 (c/cm/MeV)3 at L* = 4.2, and PSD decreased slightly with increasing L*. During this period, the LCDS was located at $L^* > 8$.

During the first compression phase (Figure 3b) the LCDS was located at L* = 5 L at the beginning of the hour, then is further compressed to L* = 3.8 by the end of the interval. PSD profiles at all μ show a clear difference between the first half hour of the interval and the latter half. In the first half hour, PSD at all μ values had a positive gradient with increasing L*, and PSD was measured at a maximum near the maximum LCDS for the interval. In the latter half hour PSD measurements are limited to $L^* < 3.8$. For μ = 900 MeV/G, PSD was measured within the minimum LCDS and was similar to the first half hour. PSD where μ = 400 MeV/G was also measured within the minimum LCDS but increased by a factor > 2 through the half hour.

392 During the net-loss phase (Figure 3c) the LCDS was located at L*~ 5.7 and remained
393 there throughout the interval. Measurements taken through the hour were co-located indicating
394 no substantial changes in PSD profiles through the interval. For both μ, the PSD peaked at L* =
395 3.8, which was the location of minimum LCDS during the compressive phase. PSD had also
396 increased by a factor of 10 or more for L* < 3.8. At L* > 3.8, PSD where μ = 400 MeV/G PSD
397 had a negative gradient with increasing L* until L* = 4.2, and PSD measurements taken by
398 GOES at L* = 5.5 were similar values to those at L* = 4.2. PSD where μ = 900 MeV/G had a
399 strong negative gradient with increasing L* > 3.8. PSD distributions presented during this net-
400 loss phase are characteristic of direct electron losses at L* > 3.8, and subsequent radial diffusion
401 after the magnetopause expanded.

402 During the secondary compression phase (Figure 3d) the LCDS was compressed at L* =
403 4.4 towards the beginning of the phase and expanded slightly to L* = 4.8 by the end of the hour.
404 PSD measurements taken throughout the hour were the constant for a given L*, showing that
405 there were no substantial changes to PSD within the hour. For both μ there were peaks in PSD at
406 L* = 3.7 with an increased PSD compared all previous intervals (Figure 3a-c). PSD at L* < 3.7
407 also increased by a factor ≥ 10 compared to the previous net-loss interval (Figure 3c) at both μ.
408 This growing peak in PSD, and increased PSD at lower L*, indicates localized electron
409 acceleration processes occurring at L* = 3.7, with radial diffusion of electrons away from this
410 location. PSD at L* > 3.7 shows that there was a strong negative gradient as PSD decreased
411 rapidly with increasing L* for both μ. PSD at these higher L* largely did not change compared
412 to the previous net-loss interval, though there were few measurements for comparison at
413 common L* between the two intervals. At L* > 4 PSD universally decreased during the second
414 compression compared to the pre-storm phase; for μ = 400 MeV/G, PSD was up to 10 times less
415 than the pre-storm interval, for μ = 900 MeV/G PSD was up to 1000 times less than the pre-
416 storm interval. In other words, despite the fact that the secondary compression phase lies within
417 the acceleration phase of this geomagnetic storm, losses at L* > 4 mean that the PSD was not
418 replenished to its pre-storm values.

4 Discussion

We presented an overview of the outer electron radiation belt response to a sequence of interacting CMEs and interplanetary shocks propagating through the solar wind in early September 2017. We used multi-mission, multi-spacecraft observations of both electron flux and phase space density to evaluate the role of magnetopause shadowing in producing changes to electron flux during this event.

Between 7 - 10 September there were two interplanetary shocks and four separate CME ejecta propagating through the solar wind. As the solar wind characteristics of this event have already been studied in detail (e.g., Scolini et al., 2020; Shen et al., 2018; Werner et al., 2019), we do not analyze these in detail, instead focusing on the relativistic electron response to these drivers. There was a complex response in electron flux at 0.8 MeV and/or 2.0 MeV energies corresponding to each interplanetary shock or CME ejecta. Most of these flux changes corresponded to changes in measurements of phase space density, indicating that the electron flux response to solar wind driving were largely due to non-adiabatic processes.

Not all changes in electron flux were due do non-adiabatic processes. Specifically, in response to the second interplanetary shock arrival, flux measured by GPS satellites decreased by orders of magnitude at all L shells. Corresponding PSD measurements showed that, whilst electrons were irreversibly lost at high L* where drift paths were intersected by the LCDS, there were initially no changes to PSD measured below L* = 3.8. Instead, the location in L* at which GPS satellites were measuring PSD changed, i.e., electron drift paths had moved radially outwards with respect to GPS orbits. Therefore, GPS satellites measured a different part of the PSD distribution, which appeared as a decrease in the measured electron flux on all L-shells. This shows why it is important to consider electron measurements in adiabatic coordinates, rather than flux alone.

We presented profiles of PSD in L* at four 1-hour time intervals in Figure 3, chosen to correspond to the four intervals depicted in Figure 2 of Turner et al. (2012). The first interval (Figure 3a) at 17:00 –18:00 UT on 6 September showed the pre-storm distribution of PSD which constantly increased with increasing L* (μ = 400 MeV/G) or reached a peak PSD at L* = 4.2 (μ = 900 MeV/G). The second interval (Figure 3b) showed PSD profiles during a high-pressure

phase at 23:00 UT 7 September to 00:00 UT 8 September, during which the magnetopause was measured by geostationary satellites. The LCDS was compressed from L* = 5 to L* = 3.8 during the hour. When the evolution of PSD within the hour was considered, we observed large scale changes to PSD as the LCDS is compressed. Electrons outside of the LCDS are no longer trapped and PSD within the LCDS in the latter half of the hour is distinctly different the pervious half hour for μ = 400 MeV/G. If we were to assume that the PSD did not change within an hour timescale, then these observations would be interpreted as false peaks or troughs in the PSD. These false peaks and troughs are produced by the dynamics of the system rather than non-adiabatic acceleration or loss processes. The third time period (Figure 3c) at 08:00 – 09:00 UT 8 September corresponded to the net-loss phase during the storm main phase. The magnetopause and LCDS had expanded outwards and there were dropouts in both electron flux at all L, and PSD at L* > 3.8. PSD profiles at all μ peaked at L* = 3.8, had increased slightly at L* < 3.8, and had decreased by orders of magnitude at L* > 3.8. This was consistent with electron loss due to direct magnetopause shadowing, followed by a redistribution of electrons via radial diffusion. The first three intervals (Figure 3a-c) correspond remarkably well to the PSD dynamics discussed by Turner et al. (2012), despite the complexity of the external solar drivers during our chosen case study.

The fourth interval (Figure 3d) does not correspond directly to the schematic in the Turner et al. (2012) study but instead corresponds to a secondary compression of the magnetosphere during the net acceleration phase between 14:00 – 15:00 UT 8 September. During this hour the magnetopause was compressed within geostationary orbit, and the LCDS was compressed to L* = 4.4. At all μ PSD increased for all L*, and there was a clear growing peak in PSD at L* = 3.7 compared to the previous time period, with strong PSD gradients across L*. This is characteristic of a localized non-adiabatic acceleration process, likely due to resonant VLF wave-particle interactions, combined with radial diffusion redistributing electrons down PSD gradients (inwards for L*<3.7 and outwards for L*>3.7), thus increasing PSD at any given L*. Furthermore, we note characteristics which suggest indirect magnetopause shadowing; strong negative gradients in PSD towards the compressed LCDS means that radial diffusion will transport particles towards the LCDS, where they will be subsequently lost. This final interval (Figure 3d) corresponds well to the PSD dynamics during indirect magnetopause shadowing discussed by Loto'aniu et al. (2010).

In order to understand how radial diffusion will have acted upon the electron populations shown in Figure 3, we use Van Allen Probe electric and magnetic field measurements to analyze power of field fluctuations. We used in-situ magnetic field observations from the Van Allen probe EMFISIS instrument (Kletzing et al., 2013) and electric field observations from the EFW instruments (Wygant et al., 2013). The magnetic and electric field measurements had a time resolution of 4 seconds. The background magnetic and electric fields were identified by taking a running average over a 20-minute sliding window, and the background fields were then subtracted from the instantaneous measurement. To identify fluctuations, the residual field observations were transformed into a magnetic field-aligned coordinate system, defined by the background magnetic field unit vector (parallel component), the geocentric position vector (azimuthal component), and the poloidal direction. In this transformed coordinate system, the parallel magnetic field perturbation and azimuthal electric field perturbation were selected to estimate the associated power spectral densities using a Morlet wavelet transform. The power spectral density was limited to a frequency range of 1-15 mHz (corresponding to the ULF wave band (Jacobs et al., 1964) and an L-range of $3 < L < 7.5$ as field perturbations cannot be reliably distinguished from the changing background field near orbital perigee.

Figure 4 shows the power spectral density of the magnetic field PB (green) and electric field PE (pink) as a function of L* for the 4 previously specified 1-hour time periods. Magnetic power spectral density is substantially enhanced at an increasing rate through the geomagnetic storm (Figure 4, panels b - d) compared to the pre-storm time period (Figure 4a). Due to data gaps in electric field measurements (associated with spacecraft charging and eclipse events), the number of electric field power spectral density measurements is variable throughout the storm, making it difficult to make comparisons between the four intervals (e.g., Figures 4 a&d). However, during the first compressive phase (Figure 4b), PE appears high with comparable, or greater, magnitudes to PB for corresponding L*. During the net-loss phase (Figure 4c), PE decreased compared to the previous compressive phase, and was less than PB at all L*. During the second compressive phase (Figure 4d), there was only one measurement of PE at L*=3.7, which was increased compared to the previous net loss phase (Figure 4c). Some of the differences between the way in which PE evolved through the intervals compared to PB may be due to changes in substorm activity affecting electric potential measured by the Van Allen Probes. Auroral geomagnetic indices (not shown) indicate enhanced substorm activity during this

interval, which will produce fluctuations in electric potential in the magnetosphere, and thus contribute towards the power spectral density of the electric field. It is therefore highly likely that PE was enhanced during interval (d) in a similar manner to interval (b). Irrespective of this, the overall rate of diffusion of the electrons is dependent on both the sum of the magnetic field and electric potential fluctuations and the PSD gradient in L*. Therefore, we conclude that outwards radial diffusion was enhanced for both intervals (c) and (d) as both periods have enhanced power spectral densities, and sharp PSD gradients in L*.

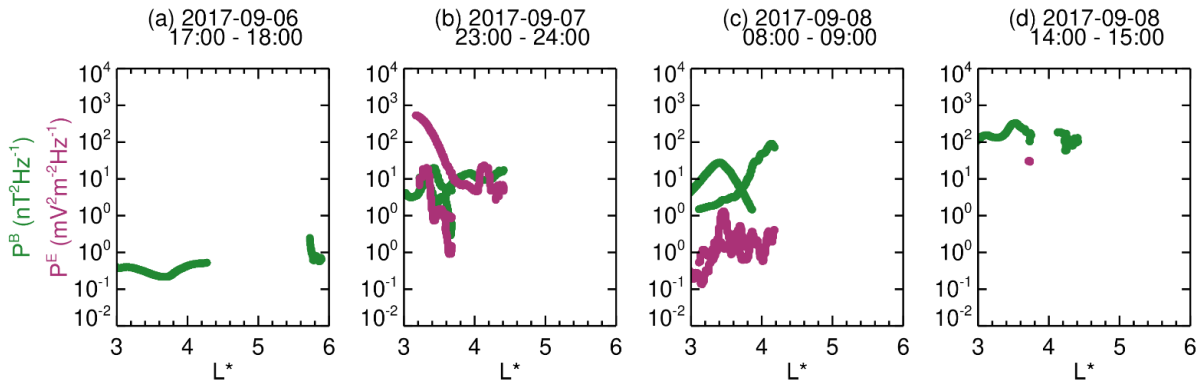

Figure 4: Estimated magnetic field (green) and electric field (purple) power spectral densities for (a) 17 - 18 UT 6th Sept, (b) 23 UT 7th - 00 UT 8th, (c) 08 – 09 UT 8th, and (d) 14 - 15 UT 8th. Each panel shows the power spectral density, summed over a frequency range of 1 to 15 mHz, plotted as a function of the L* value. Observations from both Probe A and Probe B are included.

Unfortunately, without knowing the number of particles accelerated during the local acceleration, we cannot measure the number of particles lost via indirect shadowing to evaluate the respective contributions of indirect and indirect shadowing to overall electron loss. The contributions of each mechanism could instead be estimated by replicating this event with a

Finally, we acknowledge possible limitations to this work, specifically the magnetic field model used as it is known to influence calculations of the adiabatic invariants and LCDS (e.g., Albert et al., 2018). The T01s model was chosen for this work due to its suitability during

geomagnetic storm conditions, but different magnetic field models may yield different results. Furthermore, the LCDS may be calculated by either considering Shabansky drift orbits as closed drift paths, whereas other calculations consider these bifurcating orbits as open (Öztürk & Wolf, 2007; Shabansky, 1971). In this work, we have used the last non-bifurcated drift shell as the LCDS, which could give an underestimation of the outer boundary to trapped electrons if these electrons following bifurcated orbits return to the radiation belts following the compression.

5 Summary

We used multi-point electron phase space density measurements with unprecedented temporal and spatial resolution to analyze magnetopause shadowing in the outer radiation belt during the early September 2017 geomagnetic storm. The September 2017 storm is driven by a set of complex solar wind features, due to four interacting CMEs, with an equally complex radiation belt response.

Analysis of PSD demonstrated the capabilities of multi-spacecraft measurements to identify and isolate energization and loss processes with extremely high spatial and temporal resolution:

- By comparing PSD to flux measurements we identified adiabatic transport of electrons during the event, highlighting the importance of considering adiabatic coordinates to interpret flux changes during geomagnetic storms.
- The event exhibited both similarities and differences to the Turner et al. (2012) description of an electron flux dropout. Whereas the first compression of the magnetopause showed the expected PSD responses to direct shadowing, local acceleration and additional shadowing by subsequent solar wind structures led to deviations from the Turner et al. (2012) predictions.
- We highlighted the importance of indirect magnetopause shadowing on radiation belt dynamics. Analysis of PSD and ULF wave activity showed signatures of indirect magnetopause shadowing, as described by Loto’aniu et al. (2010).

Acknowledgments

We acknowledge the developers of the IRBEM library, which was used to compute adiabatic invariant coordinates. The computations employed computational and storage services associated with the Hoffman2 Shared Cluster provided by UCLA Institute for Digital Research and Education's Research Technology Group. A. C. K. acknowledges high-performance computing support from Cheyenne (doi:10.5065/D6RX99HX) provided by NCAR's Computational and Information Systems Laboratory, sponsored by the National Science Foundation. Spacecraft data from GOES, MMS, THEMIS, and the Van Allen Probes are publicly available via the NASA/GSFC CDAWeb service (https://cdaweb.gsfc.nasa.gov/index.html/). We gratefully acknowledge the CXD team at Los Alamos National Laboratory for GPS data, which may be accessed via https://www.ngdc.noaa.gov/stp/space-weather/satellite-data/satellite-systems/gps/. Solar Wind data and geomagnetic indices are publicly available through the NASA/GSFC Space Physics Data Facility OMNIWeb service (https://omniweb.gsfc.nasa.gov/).

F. A. S. was supported by a Science and Technology Funding Council (STFC) studentship. A. C. K. was supported by NASA grants NNX16AG78G, 80NSSC20K1402, and 80NSSC20K1281. K. R. M. is partially funded by NASA ROSES Guest Investigator 18-HGIO18_2-0122 and Space Weather Operations to Research 18-HSWO2R18-0010. I. J. R. was supported by NERC Grants NE/P017185/1 and NE/V002554/1 and ST/V006320/1. J. K. S. was supported by NERC Grants NE/P017185/1 and NE/V002554/1. C.F. was supported by NERC IRF NE/N014480/1 and grants NE/P017185/1 and NE/V002554/1.

References

Albert, J. M., Selesnick, R. S., Morley, S. K., Henderson, M. G., & Kellerman,A. C. (2018). Calculation of last closed drift shells for the 2013 gem radia-tion belt challenge events. *Journal of Geophysical Research: Space Physics*, 123(11), 9597-9611. Retrieved from https://agupubs.onlinelibrary.wiley.com/doi/abs/10.1029/2018JA025991 doi: https://doi.org/10.1029/2018JA025991

590 Angelopoulos, V. (2009). The themis mission. InThe themis mission (pp. 5–34). Springer. doi:
591 https://goi.org/10.1007/s1121400893361
592
593 Angelopoulos, V., Sibeck, D., Carlson, C., McFadden, J., Larson, D., Lin, R., . . .others (2008).
594 First results from the themis mission. *Space Science Reviews*,141(1-4), 453–476. doi:
595 https://doi.org/10.1007/s11214-008-9378-4
596
597 Auster, H., Glassmeier, K., Magnes, W., Aydogar, O., Baumjohann, W., Constanti-nescu, D., . . .
598 others (2008). The themis fluxgate magnetometer. *Space sciencereviews*,141(1-4), 235–264.
599 doi: https://doi.org/10.1007/s11214-008-9365-9
600
601 Baker, D., Li, X., Blake, J., & Kanekal, S. (1998). Strong electron acceleration inthe earth's
602 magnetosphere. *Advances in Space Research*, 21(4), 609–613. Doi:
603 https://doi.org/10.1016/S0273-1177(97)00970-8
604
605 Baker, D. N., Blake, J. B., Callis, L. B., Cummings, J. R., Hovestadt, D., Kanekal,S., . . .
606 Zwickl, R. D.(1994). Relativistic electron acceleration and de-cay time scales in the inner and
607 outer radiation belts: Sampex.*Geo-physical Research Letters*, 21(6), 409-412. Retrieved from
608 https://agupubs.onlinelibrary.wiley.com/doi/abs/10.1029/93GL03532 doi:
609 https://doi.org/10.1029/93GL03532
610 Baker, D. N., Kanekal, S., Blake, J. B., Klecker, B., & Rostoker, G. (1994). Satelliteanomalies
611 linked to electron increase in the magnetosphere. *Eos, Trans-actions American Geophysical*
612 *Union*,75(35), 401-405. Retrieved from
613 https://agupubs.onlinelibrary.wiley.com/doi/abs/10.1029/94EO01038 doi:
614 https://doi.org/10.1029/94EO01038
615
616 Baker, D. N., Kanekal, S., Hoxie, V., Batiste, S., Bolton, M., Li, X., . . . others (2013). The
617 relativistic electron-proton telescope (rept) instrument on boardthe radiation belt storm probes
618 (rbsp) spacecraft: Characterization of earth'sradiation belt high-energy particle populations.
619 *Space Science Reviews*, 179(1-4), 337–381. doi: https://doi.org/10.1007/s1121401299509
620

621 Bingham, S. T., Mouikis, C. G., Kistler, L. M., Boyd, A. J., Paulson, K., Far-rugia, C. J., . . .
622 Kletzing, C.(2018).The outer radiation belt responseto the storm time development of seed
623 electrons and chorus wave ac-tivity during cme and cir driven storms. *Journal of Geophysical*
624 *Re-search: Space Physics*, 123(12), 10,139-10,157. Retrieved from
625 https://agupubs.onlinelibrary.wiley.com/doi/abs/10.1029/2018JA025963 doi:
626 https://doi.org/10.1029/2018JA025963
627
628 Blake, J., Carranza, P., Claudepierre, S., Clemmons, J., Crain, W., Dotan, Y., . . . others (2013).
629 The magnetic electron ion spectrometer (mageis) instru-ments aboard the radiation belt storm
630 probes (rbsp) spacecraft. In *The vanallen probes mission* (pp. 383–421). Springer. doi:
631 https://doi.org/10.1007/s1121401399918
632
633 Blake, J., Mauk, B., Baker, D., Carranza, P., Clemmons, J., Craft, J., . . . others (2016). The fly's
634 eye energetic particle spectrometer (feeps) sensors for themagnetospheric multiscale (mms)
635 mission. *Space Science Reviews*,199(1-4),309–329. doi: https://doi.org/10.1007/s11214-015-
636 0163-x
637
638 Borovsky, J. E., & Denton, M. H.(2009).Relativistic-electron dropouts andrecovery: A
639 superposed epoch study of the magnetosphere and the solarwind. *Journal of Geophysical*
640 *Research: Space Physics*, 114(A2). Retrieved from
641 https://agupubs.onlinelibrary.wiley.com/doi/abs/10.1029/2008JA013128 doi:
642 https://doi.org/10.1029/2008JA013128
643
644 Boscher, D., Bourdarie, S., O'Brien, P., & Guild, T. (2013). The interna-tional radiation belt
645 environment modeling (irbem) library.availableat:¡ a href=" http://sourceforge.
646 net/projects/irbem" http://sourceforge.net/projects/irbem¡/a¿ (last access: 20 August 2013).
647
648 Boyd, A. J., Spence, H. E., Claudepierre, S. G., Fennell, J. F., Blake, J. B.,Baker, D. N., . . .
649 Turner, D. L. (2014a). Quantifying the radiation beltseed population in the 17 march 2013
650 electron acceleration event. Geo-physical Research *Letters*, 41(7), 2275-2281. Retrieved from

https://agupubs.onlinelibrary.wiley.com/doi/abs/10.1002/2014GL059626 doi: https://doi.org/10.1002/2014GL059626

Boyd, A. J., Spence, H. E., Claudepierre, S. G., Fennell, J. F., Blake, J. B.,Baker, D. N., . . . Turner, D. L. (2014b). Quantifying the radiation beltseed population in the 17 march 2013 electron acceleration event. *Geo-physical Research Letters*, 41(7), 2275-2281. Retrieved from https://agupubs.onlinelibrary.wiley.com/doi/abs/10.1002/2014GL059626 doi: https://doi.org/10.1002/2014GL059626

Brautigam, D. H., & Albert, J. M. (2000). Radial diffusion analysis of outer radiation belt electrons during the october 9, 1990, magnetic storm. *Journal of Geo-physical Research: Space Physics*,105(A1), 291-309. Retrieved from https://agupubs.onlinelibrary.wiley.com/doi/abs/10.1029/1999JA900344 doi: https://doi.org/10.1029/1999JA900344

Burch, J., Moore, T., Torbert, R., & Giles, B. (2016). Magnetospheric multiscaleoverview and science objectives. *Space Science Reviews*,199(1-4), 5–21. doi: https://doi.org/10.1007/s11214-015-0164-9

Chen, Y., Friedel, R. H. W., & Reeves, G. D. (2006). Phase space density distributions of energetic electrons in the outer radiation belt during two geospaceenvironment modeling inner magnetosphere/storms selected storms. *Journalof Geophysical Research: Space Physics*, 111(A11). Retrieved from https://agupubs.onlinelibrary.wiley.com/doi/abs/10.1029/2006JA011703 doi: https://doi.org/10.1029/2006JA011703

Degeling, A. W., Ozeke, L. G., Rankin, R., Mann, I. R., & Kabin, K. (2008). Driftresonant generation of peaked relativistic electron distributions by pc 5 ulfwaves. *Journal of Geophysical Research: Space Physics*, 113(A2). Retrieved from https://agupubs.onlinelibrary.wiley.com/doi/abs/10.1029/2007JA012411 doi: https://doi.org/10.1029/2007JA012411

682

683 Dessler, A. J., & Karplus, R. (1961). Some effects of diamagnetic ring currents on van allen
684 radiation. *Journal of Geophysical Research* (1896-1977),66(8), 2289-2295. Retrieved from
685 https://agupubs.onlinelibrary.wiley.com/doi/abs/10.1029/JZ066i008p02289 doi:
686 https://doi.org/10.1029/JZ066i008p02289

687

688 Dmitriev, A. V., Suvorova, A. V., Chao, J.-K., Wang, C. B., Rastaetter, L.,Panasyuk, M. I., . . .
689 Myagkova, I. N. (2014). Anomalous dynamics of theextremely compressed magnetosphere
690 during 21 january 2005 magnetic storm. *Journal of Geophysical Research: Space Physics,*
691 119(2), 877-896. Retrieved from
692 https://agupubs.onlinelibrary.wiley.com/doi/abs/10.1002/2013JA019534 doi:
693 https://doi.org/10.1002/2013JA019534

694

695 Elkington, S. R., Hudson, M. K., & Chan, A. A. (1999). Acceleration of relativisticelectrons
696 via drift-resonant interaction with toroidal-mode pc-5 ulf oscillations. *Geophysical Research*
697 *Letters*, 26(21), 3273-3276. Retrieved from
698 https://agupubs.onlinelibrary.wiley.com/doi/abs/10.1029/1999GL003659 doi:
699 https://doi.org/10.1029/1999GL003659

700

701 Elkington, S. R., Hudson, M. K., & Chan, A. A. (2003). Resonant acceleration anddiffusion of
702 outer zone electrons in an asymmetric geomagnetic field. *Journalof Geophysical Research:*
703 *Space Physics*, 108(A3). Retrieved from
704 https://agupubs.onlinelibrary.wiley.com/doi/abs/10.1029/2001JA009202doi:https://doi.org/10.10
705 29/2001JA009202

706

707 F¨althammar, C.-G. (1965). Effects of time-dependent electric fields on geomagnetically
708 trapped radiation. *Journal of Geophysical Research* (1896-1977),70(11), 2503-2516. Retrieved
709 from https://agupubs.onlinelibrary.wiley.com/doi/abs/10.1029/JZ070i011p02503 doi:
710 https://doi.org/10.1029/JZ070i011p02503

711

712 Goes n series data book. (2010). Prepared for NASA pursuant to contract NAS5-98069.

Green, J. C., & Kivelson, M. G. (2004). Relativistic electrons in the outer radiation belt: Differentiating between acceleration mechanisms. *Journal of Geo-physical Research: Space Physics*,109(A3). Retrieved from https://agupubs.onlinelibrary.wiley.com/doi/abs/10.1029/2003JA010153 doi: https://doi.org/10.1029/2003JA010153

Green, J. C., Onsager, T. G., O'Brien, T. P., & Baker, D. N. (2004). Testing loss mechanisms capable of rapidly depleting relativistic electron flux in theearth's outer radiation belt. *Journal of Geophysical Research: Space Physics*, 109(A12). Retrieved from https://agupubs.onlinelibrary.wiley.com/doi/abs/10.1029/2004JA010579 doi: https://doi.org/10.1029/2004JA010579

Hanser, F. (2011). Eps/hepad calibration and data handbook.Tech. Rep. GOESN-ENG-048D.

Horne, R. B., Thorne, R. M., Glauert, S. A., Albert, J. M., Meredith, N. P., & An-derson, R. R. (2005). Timescale for radiation belt electron acceleration bywhistler mode chorus waves. *Journal of Geophysical Research: Space Physics*, 110(A3). Retrieved from https://agupubs.onlinelibrary.wiley.com/doi/abs/10.1029/2004JA010811 doi: https://doi.org/10.1029/2004JA010811

Horne, R. B., Thorne, R. M., Shprits, Y. Y., Meredith, N. P., Glauert, S. A., Smith,A. J., . . . others (2005). Wave acceleration of electrons in the van allen radiation belts. *Nature* ,437(7056), 227–230. doi: https://doi.org/10.1038/nature03939

Iyemori, T. (1990). Storm-time magnetospheric currents inferred from mid-latitudegeomagnetic field variations. Journal of geomagnetism and geoelectricity, 42(11), 1249–1265. doi: https://doi.org/10.5636/jgg.42.1249

Iyemori, T., Takeda, M., Nose, M., Odagi, Y., & Toh, H. (2010). Mid-latitude geomagnetic indices" asy" and" sym" for 2009 (provisional). *Data Analysis Centerfor Geomagnetism and Space Magnetism, Graduate School of Science, KyotoUniversity, Japan*.

Jacobs, J., Kato, Y., Matsushita, S., & Troitskaya, V. (1964). Classification of geomagnetic micropulsations. *Journal of Geophysical Research*, 69(1), 180–181. doi: https://doi.org/10.1029/JZ069i001p00180

Jaynes, A. N., Ali, A. F., Elkington, S. R., Malaspina, D. M., Baker, D. N., Li,X., . . . Wygant, J. R. (2018). Fast diffusion of ultrarelativistic electrons in the outer radiation belt: 17 march 2015 storm event. *Geophysical Research Letters*, 45(20), 10,874-10,882. Retrieved from https://agupubs.onlinelibrary.wiley.com/doi/abs/10.1029/2018GL079786 doi: https://doi.org/10.1029/2018GL079786

Jaynes, A. N., Baker, D. N., Singer, H. J., Rodriguez, J. V., Loto'aniu, T. M., Ali,A. F., . . . Reeves, G. D. (2015). Source and seed populations for relativistic electrons: Their roles in radiation belt changes. *Journal of Geophysical Research: Space Physics*,120(9), 7240-7254. Retrieved from https://agupubs.onlinelibrary.wiley.com/doi/abs/10.1002/2015JA021234 doi: https://doi.org/10.1002/2015JA021234

Kang, S.-B., Fok, M.-C., Komar, C., Glocer, A., Li, W., & Buzulukova, N. (2018). An energetic electron flux dropout due to magnetopause shadowing on 1 june2013. *Journal of Geophysical Research: Space Physics*,123(2), 1178-1190. Retrieved from https://agupubs.onlinelibrary.wiley.com/doi/abs/10.1002/2017JA024879 doi: https://doi.org/10.1002/2017JA024879

Kim, K. C., Lee, D.-Y., Kim, H.-J., Lyons, L. R., Lee, E. S., ̈Ozt ̈urk, M. K., & Choi,C. R. (2008). Numerical calculations of relativistic electron drift loss effect. *Journal of Geophysical Research: Space Physics*,113(A9). Retrieved from https://agupubs.onlinelibrary.wiley.com/doi/abs/10.1029/2007JA013011 doi: https://doi.org/10.1029/2007JA013011

Li, X., Baker, D. N., Temerin, M., Cayton, T. E., Reeves, E. G. D., Christensen,R. A., . . . Kanekal, S. G. (1997). Multisatellite observations of the outer zoneelectron variation during the november 3–4, 1993, magnetic storm. *Journal ofGeophysical Research: Space Physics*, 102(A7), 14123-14140. Retrieved from https://agupubs.onlinelibrary.wiley.com/doi/abs/10.1029/97JA01101 doi: https://doi.org/10.1029/97JA01101

Loto'aniu, T. M., Singer, H. J., Waters, C. L., Angelopoulos, V., Mann, I. R., Elk-ington, S. R., & Bonnell, J. W. (2010). Relativistic electron loss due to ultralow frequency waves and enhanced outward radial diffusion. *Journal of Geophysical Research: Space Physics*, 115(A12). Retrieved from https://agupubs.onlinelibrary.wiley.com/doi/abs/10.1029/2010JA015755 doi: https://doi.org/10.1029/2010JA015755

Ma, X., Xiang, Z., Ni, B., Fu, S., Cao, X., Hua, M., . . . Zhu, Q. (2020). On the loss mechanisms of radiation belt electron dropouts during the 12 september 2014 geomagnetic storm. Earth and Planetary Physics,4(6), 598-610. Retrieved from https://agupubs.onlinelibrary.wiley.com/doi/abs/10.26464/epp2020060 doi: https://doi.org/10.26464/epp2020060

Mann, I. R., Lee, E., Claudepierre, S., Fennell, J. F., Degeling, A., Rae, I., . . .others (2013). Discovery of the action of a geophysical synchrotron in the earth's van allen radiation belts. *Nature communications*, 4(1), 1–6. doi: https://doi.org/10.1038/ncomms3795

Mauk, B., Fox, N. J., Kanekal, S., Kessel, R., Sibeck, D., & Ukhorskiy, a. A. (2013). Science objectives and rationale for the radiation belt storm probes mission. *Space Science Reviews*, 179(1-4), 3–27. doi: https://doi.org/10.1007/s11214-012-9908-y

McFadden, J., Carlson, C., Larson, D., Ludlam, M., Abiad, R., Elliott, B., . . . An-gelopoulos, V. (2008). The themis esa plasma instrument and in-flight calibra-tion. *Space Science Reviews*, 141(1-4), 277–302. doi: https://doi.org/10.1007/s11214-008-9440-2

McIlwain, C. E. (1966). Ring current effects on trapped particles. *Journal of Geo-physical Research* (1896-1977),71(15), 3623-3628. Retrieved from https://agupubs.onlinelibrary.wiley.com/doi/abs/10.1029/JZ071i015p03623 doi: https://doi.org/10.1029/JZ071i015p03623

Meredith, N. P., Horne, R. B., Iles, R. H. A., Thorne, R. M., Heynderickx, D., &Anderson, R. R.(2002). Outer zone relativistic electron acceleration associated with substorm-enhanced whistler mode chorus. *Journal of Geophysical Research: Space Physics*, 107(A7), SMP 29-1-SMP 29-14. Retrieved from https://agupubs.onlinelibrary.wiley.com/doi/abs/10.1029/2001JA900146 doi: https://doi.org/10.1029/2001JA900146

Miyoshi, Y., Morioka, A., Misawa, H., Obara, T., Nagai, T., & Kasahara, Y. (2003). Rebuilding process of the outer radiation belt during the 3 november 1993 magnetic storm: Noaa and exos-d observations. *Journal of Geophysical Re-search: Space Physics*, 108(A1), SMP 3-1-SMP 3-15. Retrieved from https://agupubs.onlinelibrary.wiley.com/doi/abs/10.1029/2001JA007542 doi: https://doi.org/10.1029/2001JA007542

Miyoshi, Y., Sakaguchi, K., Shiokawa, K., Evans, D., Albert, J., Connors, M., & Jor-danova, V.(2008). Precipitation of radiation belt electrons by emic waves, observed from ground and space. *Geophysical Research Letters*, 35(23). Retrieved from https://agupubs.onlinelibrary.wiley.com/doi/abs/10.1029/2008GL035727 doi: https://doi.org/10.1029/2008GL035727

Morley, S. K., Friedel, R. H., Spanswick, E. L., Reeves, G. D., Steinberg, J. T.,Koller, J., . . . Noveroske, E. (2010). Dropouts of the outer electronradiation belt in response to solar wind stream interfaces: Global posi-tioning system observations. *Proceedings of the Royal Society A: Mathematical, Physical and Engineering Sciences*, 466(2123), 3329–3350. doi:https://doi.org/10.1098/rspa.2010.0078

Onsager, T. G., Rostoker, G., Kim, H.-J., Reeves, G. D., Obara, T., Singer, H. J.,& Smithtro, C. (2002). Radiation belt electron flux dropouts: Local time, radial, and particle-energy dependence. *Journal of Geophysical Research:Space Physics*, 107(A11), SMP 21-1-SMP 21-11. Retrieved from https://agupubs.onlinelibrary.wiley.com/doi/abs/10.1029/2001JA000187 doi: https://doi.org/10.1029/2001JA000187

Ozeke, L. G., Mann, I. R., Claudepierre, S. G., Henderson, M., Morley, S. K., Mur-phy, K. R., . . . Baker, D. N. (2019). The march 2015 superstorm revisited: Phase space density profiles and fast ulf wave diffusive transport. *Journal of Geophysical Research: Space Physics*,124(2), 1143-1156. Retrieved from https://agupubs.onlinelibrary.wiley.com/doi/abs/10.1029/2018JA026326 doi: https://doi.org/10.1029/2018JA026326

Ozeke, L. G., Mann, I. R., Olifer, L., Dufresne, K. Y., Morley, S. K., Claudepierre,S. G., . . . Degeling, A. W. (2020). Rapid outer radiation belt flux dropoutsand fast acceleration during the march 2015 and 2013 storms: The role of ultra-low frequency wave transport from a dynamic outer boundary. *Journalof Geophysical Research: Space Physics*, 125(2), e2019JA027179. Retrieved from https://agupubs.onlinelibrary.wiley.com/doi/abs/10.1029/2019JA027179(e2019JA027179 2019JA027179) doi: https://doi.org/10.1029/2019JA027179

Rae, I. J., Murphy, K. R., Watt, C. E. J., Halford, A. J., Mann, I. R., Ozeke, L. G.,. . . Singer, H. J. (2018). The role of localized compressional ultra-lowfrequency waves in energetic electron precipitation. *Journal of Geophysical Research: Space Physics*, 123(3), 1900-1914. Retrieved from https://agupubs.onlinelibrary.wiley.com/doi/abs/10.1002/2017JA024674 doi: https://doi.org/10.1002/2017JA024674

Reeves, G., Spence, H. E., Henderson, M., Morley, S., Friedel, R., Funsten, H.,. . . others (2013). Electron acceleration in the heart of the van allen radiation belts. *Science*, 341(6149), 991–994. doi: https://doi.org/10.1126/science.1237743

Reeves, G. D., McAdams, K. L., Friedel, R. H. W., & O'Brien, T. P.(2003). Acceleration and loss of relativistic electrons during geomagnetic storms. *Geophysical Research Letters*, 30(10). Retrieved from https://agupubs.onlinelibrary.wiley.com/doi/abs/10.1029/2002GL016513 doi: https://doi.org/10.1029/2002GL016513

Rodger, C. J., Hendry, A. T., Clilverd, M. A., Kletzing, C. A., Brundell, J. B.,& Reeves, G. D. (2015). High-resolution in situ observations of electronprecipitation-causing emic waves. *Geophysical Research Letters*, 42(22), 9633-9641. Retrieved from https://agupubs.onlinelibrary.wiley.com/doi/abs/10.1002/2015GL066581 doi: https://doi.org/10.1002/2015GL066581

Rodger, C. J., Turner, D. L., Clilverd, M. A., & Hendry, A. T.(2019). Magnetic local time-resolved examination of radiation belt dynamics during high-speed solar wind speed-triggered substorm clusters. *Geophys-ical Research Letters*, 46(17-18), 10219-10229. Retrieved from https://agupubs.onlinelibrary.wiley.com/doi/abs/10.1029/2019GL083712 doi: https://doi.org/10.1029/2019GL083712

Rodriguez, J. V., Krosschell, J. C., & Green, J. C.(2014). Intercalibration of goes 8–15 solar proton detectors. *Space Weather*, 12(1), 92-109. Retrieved from https://agupubs.onlinelibrary.wiley.com/doi/abs/10.1002/2013SW000996 doi: https://doi.org/10.1002/2013SW000996

Roederer, J. (1970). Dynamics of geomagnetically trapped radiation.

Saito, S., Miyoshi, Y., & Seki, K.(2010). A split in the outer radiation belt by magnetopause shadowing: Test particle simulations. *Journal of Geo-physical Research: Space Physics*,115(A8). Retrieved from https://agupubs.onlinelibrary.wiley.com/doi/abs/10.1029/2009JA014738 doi: https://doi.org/10.1029/2009JA014738

Schulz, M., & Lanzerotti, L. J.(1974). Adiabatic invariants and magnetosphericmodels. In Particle diffusion in the radiation belts (pp. 10–45). *Springer*. doi: https://doi.org/10.1007/978-3-642-65675-02

Scolini, C., Chan´e, E., Temmer, M., Kilpua, E. K., Dissauer, K., Veronig, A. M., . . .others (2020). Cme–cme interactions as sources of cme geoeffectiveness: Theformation of the complex ejecta and intense geomagnetic storm in 2017 earlyseptember. *The Astrophysical Journal Supplement Series*, 247(1), 21.doi: https://doi.org/10.3847/1538-4365/ab6216

Selesnick, R. S., & Blake, J. B. (2000). On the source location of radiation beltrelativistic electrons. *Journal of Geophysical Research: Space Physics*, 105(A2), 2607-2624. Retrieved from https://agupubs.onlinelibrary.wiley.com/doi/abs/10.1029/1999JA900445 doi: https://doi.org/10.1029/1999JA900445

Shabansky, V. (1971). Some processes in the magnetosphere. *Space Science Reviews*,12(3), 299–418.

Shen, C., Xu, M., Wang, Y., Chi, Y., & Luo, B.(2018). Why the shock-icmecomplex structure is important: Learning from the early 2017 september cmes.*The Astrophysical Journal*,861(1), 28. doi: https://doi.org/10.3847/1538-4357/aac204

Shprits, Y., Daae, M., & Ni, B.(2012). Statistical analysis of phase space density buildups and dropouts. *Journal of Geophysical Research: Space Physics*, 117(A1). Retrieved from https://agupubs.onlinelibrary.wiley.com/doi/abs/10.1029/2011JA016939 doi: https://doi.org/10.1029/2011JA016939

Shprits, Y. Y., Thorne, R. M., Friedel, R., Reeves, G. D., Fennell, J., Baker, D. N.,& Kanekal, S. G. (2006). Outward radial diffusion driven by losses at magnetopause. *Journal of Geophysical Research: Space Physics*, 111(A11). Retrieved from https://agupubs.onlinelibrary.wiley.com/doi/abs/10.1029/2006JA011657 doi: https://doi.org/10.1029/2006JA011657

Shue, J.-H., Song, P., Russell, C., Steinberg, J., Chao, J., Zastenker, G., . . . others (1998). Magnetopause location under extreme solar wind conditions. *Journal of Geophysical Research: Space Physics*,103(A8), 17691–17700. doi: https://doi.org/10.1029/98JA01103

Sibeck, D. G., Baumjohann, W., Elphic, R. C., Fairfield, D. H., Fennell, J. F., Gail,W. B., . . . Takahashi, K. (1989). The magnetospheric response to 8-minuteperiod strong-amplitude upstream pressure variations. *Journal of Geophysical Research: Space Physics*, 94(A3), 2505-2519. Retrieved from https://agupubs.onlinelibrary.wiley.com/doi/abs/10.1029/JA094iA03p02505 doi: https://doi.org/10.1029/JA094iA03p02505

Sibeck, D. G., McEntire, R. W., Lui, A. T. Y., Lopez, R. E., & Krimigis, S. M. (1987). Magnetic field drift shell splitting: Cause of unusual dayside particle pitch angle distributions during storms and substorms. Journal of Geophysical Research: Space Physics,92(A12), 13485-13497.Retrieved from https://agupubs.onlinelibrary.wiley.com/doi/abs/10.1029/JA092iA12p13485 doi: https://doi.org/10.1029/JA092iA12p13485

Singer, H., Matheson, L., Grubb, R., Newman, A., & Bouwer, D. (1996). Monitoring space weather with the goes magnetometers. In Goes-8 and beyond (Vol. 2812,pp. 299–308).

Staples, F. A., Rae, I. J., Forsyth, C., Smith, A. R. A., Murphy, K. R., Raymer,K. M., . . . Imber, S. M.(2020). Do statistical models capture the dynamics of the magnetopause during sudden magnetospheric compressions? *Journal of Geophysical Research: Space Physics*, 125(4), e2019JA027289. Retrieved from https://agupubs.onlinelibrary.wiley.com/doi/abs/10.1029/2019JA027289(e2019JA027289 10.1029/2019JA027289) doi: https://doi.org/10.1029/2019JA027289

Summers, D., Thorne, R. M., & Xiao, F.(1998).Relativistic theory of wave-particle resonant diffusion with application to electron acceleration in themagnetosphere. *Journal of Geophysical*

Research: Space Physics, 103(A9),20487-20500. Retrieved from https://agupubs.onlinelibrary.wiley.com/doi/abs/10.1029/98JA01740 doi: https://doi.org/10.1029/98JA01740

Thorne, R. M., & Kennel, C. F.(1971). Relativistic electron precipitation duringmagnetic storm main phase. *Journal of Geophysical Research* (1896-1977),76(19), 4446-4453. Retrieved from https://agupubs.onlinelibrary.wiley.com/doi/abs/10.1029/JA076i019p04446 doi: https://doi.org/10.1029/JA076i019p04446

Tsyganenko, N. A., Singer, H. J., & Kasper, J. C.(2003).Storm-time distor-tion of the inner magnetosphere: How severe can it get? *Journal of Geophysical Research: Space Physics*,108(A5). Retrieved from https://agupubs.onlinelibrary.wiley.com/doi/abs/10.1029/2002JA009808 doi: https://doi.org/10.1029/2002JA009808

Tu, W., Xiang, Z., & Morley, S. K. (2019). Modeling the magnetopause shadowing loss during the june 2015 dropout event. *Geophysical Research Letters*, 46(16), 9388-9396. Retrieved from https://agupubs.onlinelibrary.wiley.com/doi/abs/10.1029/2019GL084419 doi: https://doi.org/10.1029/2019GL084419

Turner, D. L., Angelopoulos, V., Li, W., Hartinger, M. D., Usanova, M., Mann,I. R., . . . Shprits, Y. (2013). On the storm-time evolution of relativis-tic electron phase space density in earth's outer radiation belt. *Journal ofGeophysical Research: Space Physics*, 118(5), 2196-2212. Retrieved from https://agupubs.onlinelibrary.wiley.com/doi/abs/10.1002/jgra.50151 doi: https://doi.org/10.1002/jgra.50151

Turner, D. L., Shprits, Y., Hartinger, M., & Angelopoulos, V. (2012). Explaining sudden losses of outer radiation belt electrons during geomagnetic storms. *Nature Physics*, 8(3), 208–212. doi: https://doi.org/10.1038/nphys2185

Tuszewski, M., Cayton, T. E., Ingraham, J. C., & Kippen, R. M. (2004). Bremsstrahlung effects in energetic particle detectors.Space Weather, 2(10). Retrieved from https://agupubs.onlinelibrary.wiley.com/doi/abs/10.1029/2003SW000057 doi: https://doi.org/10.1029/2003SW000057

Wanliss, J. A., & Showalter, K. M. (2006). High-resolution global storm index: Dst versus sym-h. *Journal of Geophysical Research: Space Physics*, 111(A2). Retrieved from https://agupubs.onlinelibrary.wiley.com/doi/abs/10.1029/2005JA011034 doi: https://doi.org/10.1029/2005JA011034

Werner, A. L. E., Yordanova, E., Dimmock, A. P., & Temmer, M. (2019). Modeling the multiple cme interaction event on 6–9 september 2017 with wsa-enlil+cone. *Space Weather*, 17(2), 357-369.Retrieved from https://agupubs.onlinelibrary.wiley.com/doi/abs/10.1029/2018SW001993 doi:https://doi.org/10.1029/2018SW001993

Wrenn, G., Rodgers, D., & Ryden, K. (2002). A solar cycle of spacecraft anomalies due to internal charging. In Annales geophysicae (Vol. 20, pp. 953–956). doi: https://doi.org/10.5194/angeo-20-953-2002,2002

Wrenn, G. L. (1995). Conclusive evidence for internal dielectric charging anomalieson geosynchronous communications spacecraft. *Journal of Spacecraft and Rockets*, 32(3), 514–520. doi: https://doi.org/10.2514/3.26645

Xiang, Z., Tu, W., Li, X., Ni, B., Morley, S. K., & Baker, D. N. (2017). Understanding the mechanisms of radiation belt dropouts observed by Van Allen Probes. *Journal of Geophysical Research: Space Physics*, 122, 9858– 9879. doi: https://doi.org/10.1002/2017JA024487

Zou, Z., Zuo, P., Ni, B., Gao, Z., Wang, G., Zhao, Z., . . . Wei, F. (2020). Two-step dropouts of radiation belt electron phase space density induced by amagnetic cloud event. *The Astrophysical Journal Letters*, 895(1), L24. doi: https://doi.org/10.3847/2041-8213/ab9179

1018 Oztˇurk, M. K., & Wolf, R. A. (2007). Bifurcation of drift shells near the dayside magnetopause.
1019 *Journal of Geophysical Research: Space Physics*, 112(A7). Retrieved from
1020 https://agupubs.onlinelibrary.wiley.com/doi/abs/10.1029/2006JA012102 doi:
1021 https://doi.org/10.1029/2006JA012102